Mid-infrared ultra-short pulse generation in a gas filled hollow-core fiber pumped by two pulses

Coralie Fourcade-Dutin, Olivia Zurita Miranda, Patrick Mounaix, Damien Bigourd

Article

Mid-infrared ultra-short pulse generation in a gas-filled hollow-core fiber pumped by two pulses [Invited].

Coralie Fourcade-Dutin [1,*], Olivia Zurita Miranda [1,2], Patrick Mounaix [1] and Damien Bigourd [1, **]

[1] Laboratoire IMS, UMR CNRS 5218, University of Bordeaux, 33400 Talence, France; [2] Institut FEMTO-ST, Département d'Optique, UMR CNRS 6174 -Université Bourgogne Franche-Comté, 25030 Besançon, France
* Correspondence: coralie.fourcade-dutin@u-bordeaux.fr;
** Correspondence: damien.bigourd@u-bordeaux.fr;

Received: date; Accepted: date; Published: date

Abstract: We show that ultra-short pulses can be generated in the mid-infrared when a gas filled hollow-core fiber is pumped by a fundamental pulse and its second harmonic. The generation process originates from cascaded nonlinear phenomenon starting from a spectral broadening of the two pulses followed by an induced phase-matched four wave-mixing lying in the mid-infrared combined with a dispersive wave. By selecting this mid-infrared band with a spectral filter, we demonstrate the generation of ultra-short 60 fs pulses at 3-4 μm band and a pulse duration of 20 fs can be reached with additional phase compensator.

Keywords: Mid-infrared pulse generation, Four-wave mixing, Anti-resonant hollow-core fiber

1. Introduction

Since these recent years, an interest is growing for the mid-infrared (MIR) sources driven by demanding applications as gas sensing [1], food inspection [2], life and molecular sciences [3] or the creation of secondary sources [4]. An excellent method for the light generation in the MIR is to combine some laser properties with nonlinear photonic devices to create down-converted frequencies. For example, high power sources can be made from several efficient nonlinear crystals, chosen from their optimal phase matching conditions and absorption bands to achieve an optical parametric amplification effect or difference frequency generation. Other few alternative devices at lower power are based on other transparent materials as in silicon-, lithium niobate- or chalcogenide-based waveguides [5-7] or specific nonlinear fibers with soft-glass materials [8].

In this manuscript, we propose to generate ultra-short pulses in the MIR by pumping a gas-filled hollow-core photonic crystal fiber (HC-PCF) with two different pulses to create an efficient phase-matched process. The HC-PCFs bring significant advantages to handle and convert ultra-short pulses. Particularly, they offer a high damage threshold which allows the propagation of high peak power [9]. In addition, the frequency conversion from the pump to the MIR can be engineered with the dispersion of the waveguide and the gas contribution, i.e the phase matching can be tuned in real time by changing the gas pressure. Outstanding progresses have also been achieved to reduce the loss of HC-PCFs in the MIR [10,11], for example, with a transmission loss of ~25-50 dB/km now being obtained by minimizing the interaction between the core guided mode and the silica walls of the cladding of an inhibited-coupling hollow-core fiber [10]. Recent anti-resonant HC-PCFs have also gained interest [12] due to their properties including a wide tunability of the spectral transmission bands from the Ultra-violet (UV) to MIR [13,14,15] with low loss, high damage threshold [16] and a single mode propagation by choosing specific geometries [17]. Several impressive works on ultra-short pulse generation in the MIR with gas filled HC-PCFs have been reported, such as pulse compression [18], supercontinuum and MIR dispersive wave generation [13,19,20] and adiabatic

down conversion from four wave mixing (FWM) processes in a tapered fiber [21]. In this later case, the HC-PCF is pumped by two picosecond pulses and seeded with a chirped signal to overlap with the conversion spectral band. In our approach, only two ultra-short pump pulses are injected and spectrally broadened in the HC-PCF. FWM are directly induced from the two broad-band pulses capable to generate pulses at 3 and 4 μm with a duration of 20 fs.

2. Anti-resonant fibers and numerical methods

2.1. Properties of the hollow-core photonic crystal fiber

The chosen HC-PCF geometry is a negative curvature fiber based on a single-ring structure surrounding by the hollow-core. This type of fiber generally supports a large family of high-order modes but in a specific condition (d=0.68D with d and D the tube and core diameters, respectively), it can provide a single mode LP_{01} operation [17]. A schematic view is shown in the inset of Figure 1 with our chosen parameters.

The HC-PCF structure is composed of a central hollow core with D=150 μm surrounded by seven evenly and non-touching capillaries attached to the inner surface of a thick-walled capillary. The tube diameter is set at 102 μm to ensure a robust single-mode propagation. The wall thickness t equals to 0.2 μm and the gap between tube g equals to 7.3 μm. The LP_{01} mode at 1030 nm supported by this HC-PCF has also been simulated by the finite element method (insert in Figure 1) and it also confirms the great advantage to propagate waves in the MIR with low loss since the overlap of the spatial profile with the silica structure is weak even if the glass is highly absorbent in the MIR.

The group velocity dispersion, β_2, is firstly analytically calculated for the fundamental mode from empirical formulae [22] derived from a modification of the Marcatelli and Schmelzer's capillary model [23] to take into account the anti-resonant reflection. Figure 1 shows the dispersion curve as a function of the wavelength for an HC-PCF filled with argon at a pressure of 5 bar. This pressure is chosen to obtain a zero-dispersion wavelength (ZDW) in the near infrared at 1170 nm. The effective area A_{eff} ~992 μm^2 is also calculated from the model [22] and is assumed constant for the spectral range.

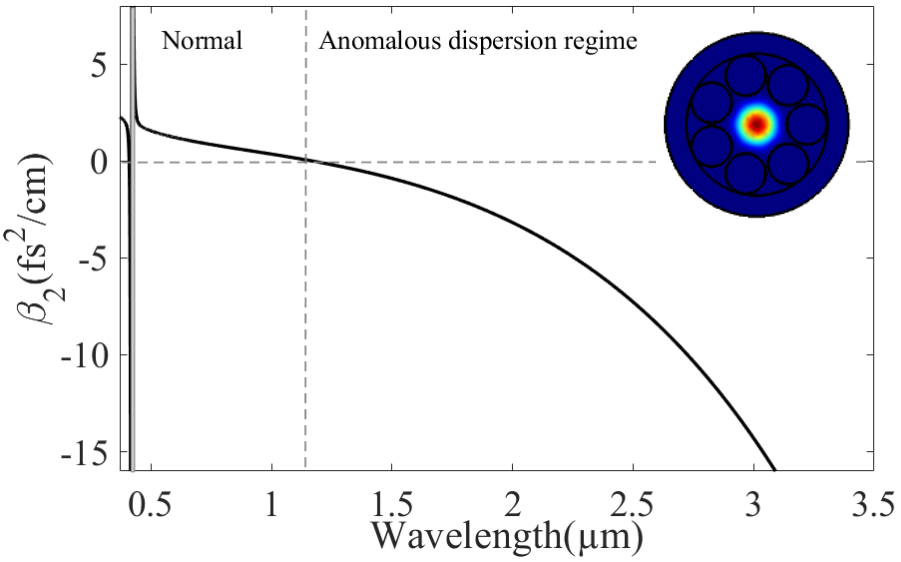

Figure 1. Group velocity dispersion as a function of the wavelength for the HC-PCF filled with argon at a pressure of 5 bar. The grey area represents the resonant band. The inset represents a schematic view of the fiber with the LP_{01} mode t 1030 nm.

2.2. Numerical method for the nonlinear pulse propagation

The general principle for MIR generation is to pump the HC-PCF with two different ultra-short pulses, P1 and P2, with spectra centered at 1030 nm and 515 nm corresponding to the emission of an ultra-fast ytterbium doped fiber laser and a second harmonic generator. The two pulses lie in the normal dispersion regime and the spectra broaden during the propagation in the fiber. Then, the MIR light is generated from a phase matched FWM between several created spectral components. In order to deeply understand the concept and the dynamics, we conducted numerical simulations by integrating the generalized nonlinear Schrödinger equation

$$\frac{\partial A}{\partial z} - \sum_{n\geq 2} \frac{i^{n+1}}{n!} \beta_n \frac{\partial^n A}{\partial T^n} = i\gamma\left(1 + i\tau_{shock} \frac{\partial}{\partial T}\right)\left|A\right|^2 A \quad (1)$$

describing the evolution along the fiber length z of the complex total electric field A(z,T).

The initial field corresponds to the total field composed of P1 and P2; i.e

$$A(z=0,T) = A_1 \exp(i(\omega_1 - \omega_c).T) + A_2 \exp(i(\omega_2 - \omega_c).T) \quad (2)$$

ω_1 (ω_2) and A_1 (A_2) are the angular frequency and the electric field amplitude of the pump P1 (P2), respectively. In our simulation, we choose to center the frequency grid between the two pumps; at ω_c corresponding to a wavelength of ~686 nm. Accordingly, we choose T in equation (1) as the time in the frame moving at the group velocity β_{1c} at ω_c.

The series expansion coefficient of the dispersion term β is calculated in the frequency domain from the empirical model (section 2.1) . The time derivative in the right-hand side is important to take into account the shock term on a time scale of $\tau_{shock} = \frac{1}{\omega_c} - \left[\frac{1}{n_{eff}(\omega)} \frac{\partial n_{eff}(\omega)}{\partial \omega}\right]_{\omega c}$ [24]. γ is the nonlinear term allowing to generate the new frequency components according to $\gamma = \frac{\omega_c \cdot n_2}{A_{eff}.c}$ with n_2 the argon nonlinear index equals to 4.86 x 10^{-23} m^2/W and c, the speed of light.

3. Continuum generation

3.1. Generated continuum from a dual-pump scheme

The light is generated in the MIR from a cascade of nonlinear processes in the argon filled HC-PCF pumped by the two pump pulses. The initial pulses P_1 and P_2 have a duration of 180 fs and 50 fs at Full-Width at Half Maximum (FWHM) at the Fourier transform limit. The corresponding spectral bandwidth are $\Delta\lambda_1$~9 nm and $\Delta\lambda_2$~8 nm at FWHM . The group delay mismatch (GDM) between the two pulses is ~176 fs/m (Figure 2.a) and we consider a total fiber length of 50 cm to ensure a temporal overlap during the propagation. At the input fiber, the energies are 12 μJ for P_1 and 20 μJ for P_2 such as the peak powers reach 63 MW and 390 MW. At first, each spectrum broadens along the fiber. Figure 2.b shows the spectra for a 50 cm long fiber (black solid-line). For comparison, the spectra are also displayed when only P_1 (red dashed-line) or P_2 (red dotted-line) is injected in the HC-PCF. Clearly, the spectral broadening of P_2 is mostly due to self-phase modulation (SPM) since P_1 does not affect significantly the spectral shape; i.e the spectra are similar with or without P1. Alternatively, SPM has a negligible contribution on P_1 and the phase modulation on P_1 is induced by P_2. This cross phase modulation (XPM) allows to generate a broad-bandwidth centered at 1030 nm even for a weaker pulse P_1 [25].

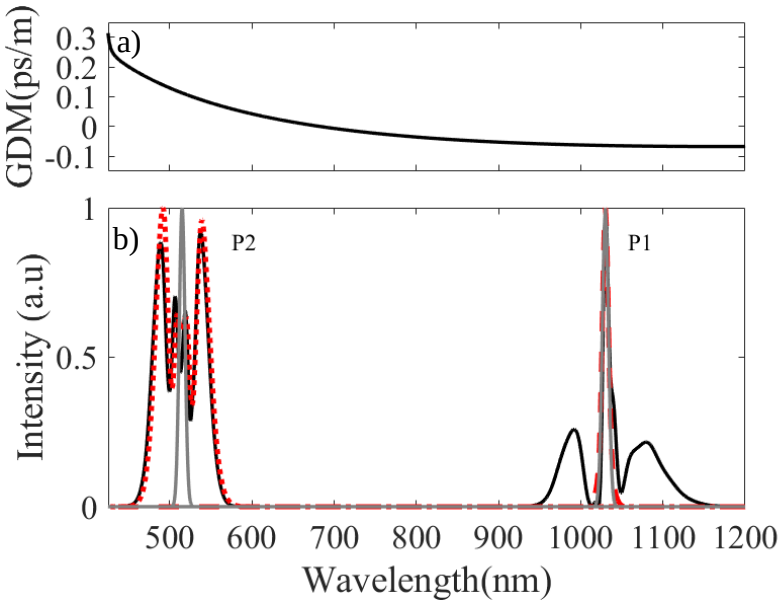

Figure 2. (**a**) Group delay mismatch as a function of the wavelength. (b) Output spectrum for L=50 cm when P_1 (red dashed-line), P_2 (red dotted-line) or both pulses (black solid-line) are injected in the 50 cm long HC-PCF. The input spectra are also displayed (grey solid-lines).

3.2. Frequency generation mechanism and dynamics

Figure 3 displays the total spectrum as a function of the fiber length with a logarithmic scale. During the pulse propagation, the two pumps symmetrically undergo spectral broadenings due to the phase modulations and a portion of the pump energy enters in the anomalous dispersion regime at z~10 cm. In addition, the spectral tail of the broadened pulse P_2 extends and overlaps with phase matched frequencies in which the energy transfer process takes place. Other spectral components are generated in the UV at ~374 nm (zone 1), in the near-IR (zone 2) and MIR (zone 3) due to the interaction of the two main pulses with a large spectral bandwidth to achieve phase match processes mostly from a FWM. For example, the radiation at (zone 1) results from the FWM process between the pump (P_2) seeded with P_1 leading to an angular frequency of $2.\omega_2-\omega_1$.

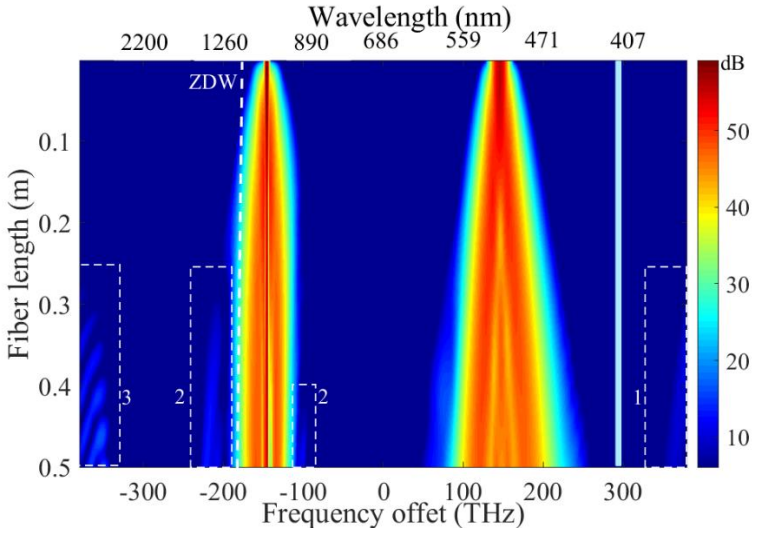

Figure 3. Total spectrum as a function of the fiber length with a logarithmic scale. Zone 1, 2 and 3 correspond to some generated bands in the UV, near IR and MIR. The light-blue line represents the absorption band of the HC-PCF.

The other FWMs relies on a degenerated phase-matched process involving one strong pump pulse (i.e P_1) and a weak wave, at the angular frequency ω_s, which is originated from the broadening of the second pulse P_2. One idler band is generated in the MIR at the angular frequency ω_i, and then it will be selected with band-pass filters. In order to reach an ultrashort pulse, a broad-band FWM is required and we take benefit from a pump pulse (P_1) with a broad spectral bandwidth [26,27]. The phase-matching condition inside the HC-PCF, κ, is defined by the sum of a linear contribution that depends on the properties of the fiber,the gas and a nonlinear term :

$$\kappa = \left\{2\beta_p(\omega_1) - \beta_s(\omega_s) - \beta_i(\omega_i)\right\} + 2\gamma P_{P1} \quad (3)$$

With $\beta_{p,s,i}$ the wave vector of each photon (pump, signal, idler) and P_{p1} the pump peak power. Figure 4 correspond to the analytically calculated coherence length, i.e $1/\kappa$, as the function of the pump wavelength. This wavelength range corresponds to the bandwidth of the pulse P_1. For this estimation, the peak power P_{p1} is kept constant (W) although the instanstaneous power variation modifies the phase matching condition.

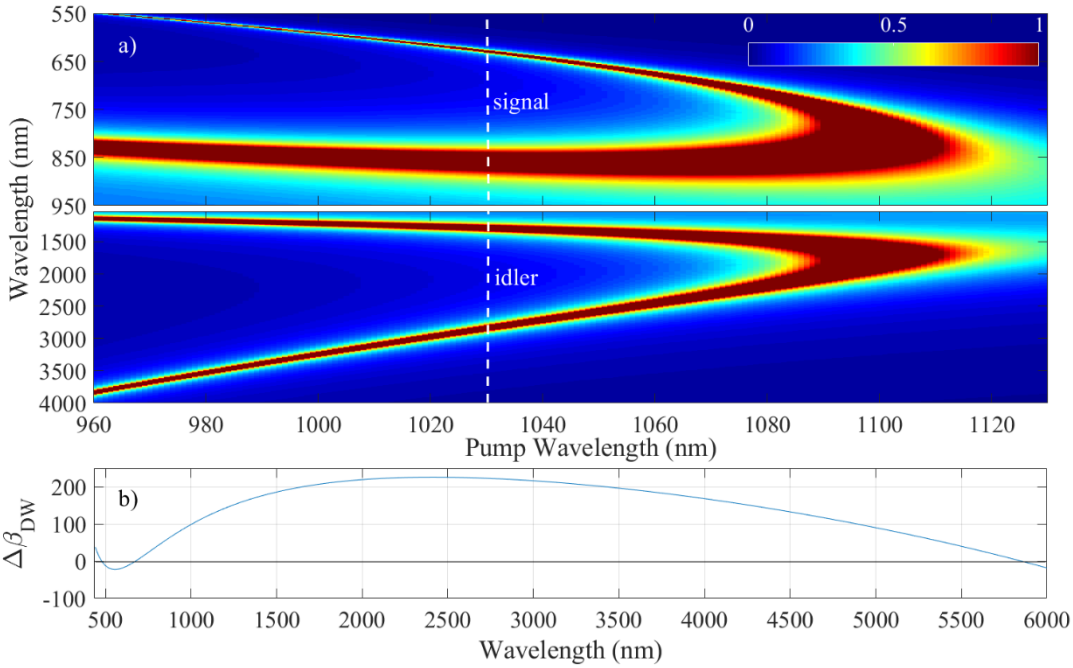

Figure 4. (**a**) Coherence length ($1/\kappa$) as a function of the pump P_1 wavelength for a constant peak power of 63 MW (from Eq. 3). (**b**) Phase mismatch of the dispersive wave ($\Delta\beta_{DW}$) as a function of the wavelength for the pump P_2 (from Eq. 4).

The coherence length is maximum when the pump wavelength lies in the normal dispersion regime ($\beta_2>0$) and only a part of the P_1 spectrum plays a role in the FWM. Several bands arise around the pump wavelengths. For example, two side-band pairs (signal/idler) are located at 0.85/1.2 µm and 0.62/2.8 µm for a pump wavelength sets at 1030 nm (vertical white lines in Figure 4.a). The locations of these bands are in good agreement with those observed in the numerical simulations (zone 2 and 3, Figure 3). In addition, it is important to note that the visible band overlaps with the spectrum of P_2 that allows to generate the MIR band. The MIR spectrum obtained from the numerical simulations (Figure 3) is displayed in Figure 5. It has a bandwidth (FWHM) of 1000 nm and exhibits several lobes with maxima at 3.4 and 4.2 µm. This structure is probably due to the modulated spectrum of P_1 that directly influences the shape of the band [26].

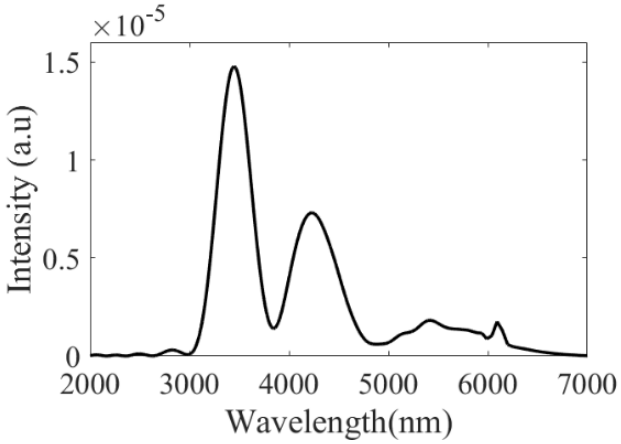

Figure 5. MIR spectrum at the HC-PCF output.

In addition to this wide spectral band, we can also note that a weaker peak arises at ~5.5 μm defined as a dispersive wave (DW) seeded by spectral tail of the FWM band. This separate sideband radiation lies in the anomalous dispersion regime and is resonantly amplified by the pulse P_2 in the normal dispersion regime [20,28], according to the phase matching condition of the DW given by [19] :

$$\Delta\beta_{DW} = \beta(\omega) - \left\{ \beta(\omega_2) + \beta_1(\omega_2)\left[\omega - \omega_2\right] + \gamma P_{p2}\left[\frac{\omega}{\omega_2}\right] \right\} \quad (4)$$

with P_{p2} is peak power of P_2. This phase-mismatch is plotted in Figure 4.b. The perfect phase-matching is obtained when $\Delta\beta_{DW}$ becomes zero at 5.8 μm in good agreement with the observed weak MIR band (Figure 5).

As observed in Figure 3, the MIR band is only efficiently generated when the signal at ~620 nm is created from the early-spectral broadening process of P_2. Firstly, the P_2 spectrum broadens during propagation due to SPM and at ~30 cm (Figure 3), the spectral tail reaches the visible band of the FWM and MIR waves are generated. In Figure 3, we also observed that the band at 1.2 μm arises at z~30 cm once the signal at 850 nm arises from the spectral broadening of P_1. This MIR band evolves during the propagation in the HC-PCF and their origins can be also discussed from the spectrogram (Figure 6) where we show the time-frequency distribution of the total field at the fiber output. During the propagation, the two pulses accumulated some temporal phase and therefore the instantaneous frequencies is quasi-linearly spread in time. As the spectral broadening of P_1 is due to the XPM with P_2, this chirp is only observed during the pulse overlap. Similarly, the additional bands (in the UV, NIR and MIR) can be generated only once the two pumps overlap. Each pulse owns a defined spectral bandwidth that evolves along the fiber (Figure 3). From Figure 6, we can also observe that the MIR band has a spectro-temporal distribution. In fact, the pump and signal chirps are transferred to the idler [27] creating the spectro-temporal distribution [26, 29].

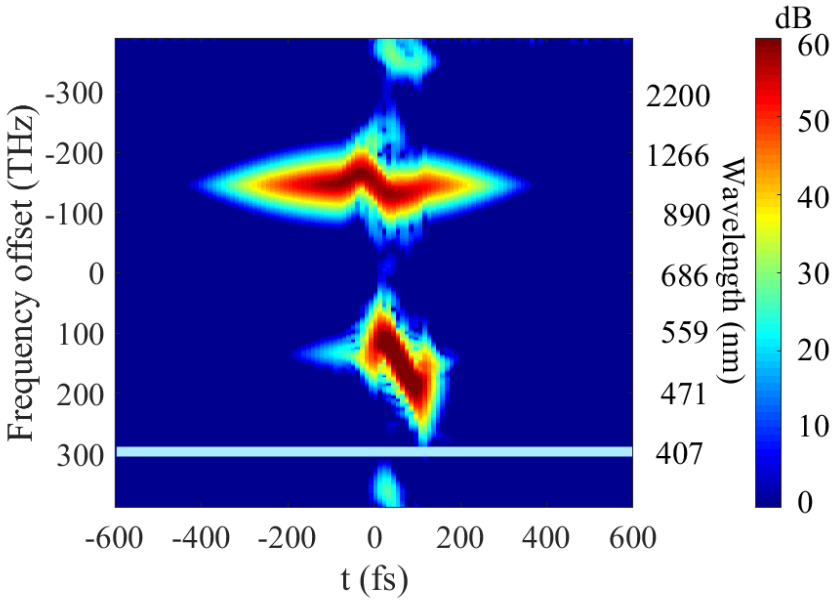

Figure 6. Spectrogram at the output HC-PCF. The light-blue line represents the absorption band of the HC-PCF.

3.3 Pulse properties of the filtered mid-infrared continuum

At the output of the HC-PCF, the MIR band is selected with a flat-top bandpass filter and the pulse shape is directly calculated. By selecting the MIR band between 3 and 5 μm , the temporal shape exhibits two peaks separated by 48 fs (blak solid-line in Figure 5). This structured temporal profile is dued to the uncompensated phase acquired during the propagation and the nonlinear conversion in the fiber. At the HC-PCF output, the accumulated phase can be compensated in order to reach an ultra-short pulse duration of ~20 fs (grey solid-line). When each lobes are filtered, the temporal profile has a bell-shape with a duration of ~60 fs at 3.4 μm or 4.2 μm without any phase conpensation (black dashed and dotted-lines-Figure 3). An energy of few nJ is obtained at the fiber output. Therefore, this scheme is highly desirable to develop a simple and robust pre-amplifier to seed subsequent ultra-fast amplifier in the MIR.

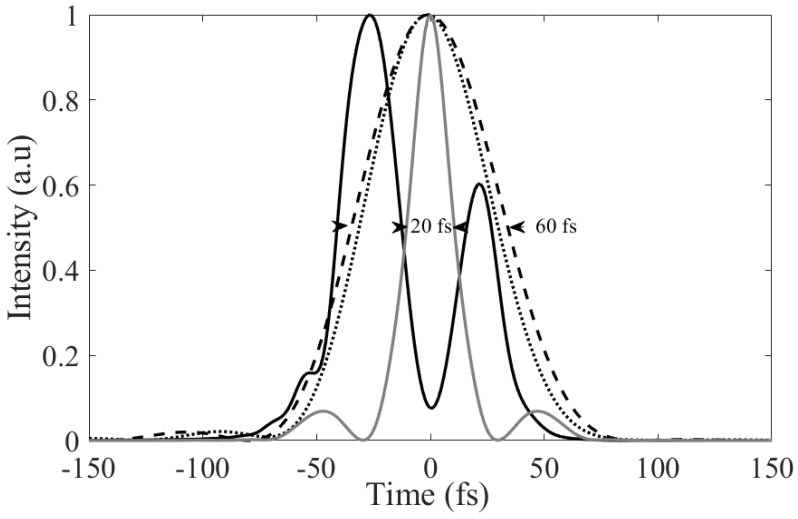

Figure 7. Temporal profiles of the MIR band (black solid-line) and filtered spectra at 3.4 μm or 4.2 μm (black dashed or dotted line). The grey solid-line corresponds to the pulse profile without the filter when the total phase is compensated.

5. Conclusion

We numerically demonstrated that ultra-short pulses at 3 and 4 μm can be generated through the interaction of a fundamental pulse and its harmonics in a HC-PCF filled with argon. The generation process originates from cascaded nonlinear phenomenon starting from spectral broadening of the two pulses followed by an induced phase-matched four wave-mixing. The selected MIR band can directly provide sub-60 fs pulses and a duration of ~20 fs is expected if a system of phase compensation is used. This technique can be easily implemented since it relies on available laser systems and state of the art anti-resonant fibers. The method is very promising to access the MIR spectral ranges in the ultra-short pulse regime in a robust fiber system.

Author Contributions: C. F-D., O Z-M. and D.B. conceived, developed the model and performed the full simulation; C.F-D and D.B analyzed the data and wrote the manuscript. D.B and PM supported this project. PM, O. Z-M discussed the results, and reviewed the manuscript.

Funding: This research was funded by the ANR (ANR-10-IDEX-03-02, ANR-17-EURE-0002,) and Bourgogne Franche-Comté council (SUM Project).

Conflicts of Interest: "The authors declare no conflict of interest."

References

1. Woodward, R.I.; Majewski, M.R.; Hudson, D.D; Jackson, S.D. Swept-wavelength mid-infrared fiber laser for real-time ammonia gas sensing. *APL Photonics* **2019**, *4*, 020801.
2. Baldauf, N.A.; Rodriguez-Romo, L.A.; Yousef, A.E; Rodriguez-Saona, L.E. Serovars by Fourier transform mid-infrared spectrocopy. *Appl. Spec.* **2006**, *60*, 592-598.
3. Müller-Werkmeister, H.M.; Li, Y-L.; Lerch, E-B.W; Bigourd, D.; Bredenbeck, J. Ultrafast hopping from band to band: Assigning infrared spectra based on vibrational energy transfer. *Angewandte IE Chemie* **2013**, *52*, 6214-6217.
4. Koulouklidis, D.A.; Gollner, C.; Shumakova, V.; Fedorov, V.Y.; Pugžlys, A.; Baltuška, A.; Tzortzakis, S. Observation of extremely efficient terahertz generation from mid-infrared two-color laser filaments. *Nat. Comm.* **2020**, 11, 292.
5. Zlatanovic, S.; Park, J.S.; Moro, S.; Chavez Boggio, J.M.; Divliansky, I.B.; Alic, N.; Mookherjea S.; Radic S. Mid-infrared wavelength conversion in silicon waveguides using ultra-compact telecom-band-derived pump source. *Nat. Phot.* **2010**, 4, 561-564.
6. Kowligy, S.A.; Lind, A.; Hickstein, D.D.; Carlson, D.R.; Timmers, H.; Nader, N.; Cruz, F.C.; Ycas, G.; Papp, S.B.; Diddams, S.A. Mid-infrared frequency comb generation via cascaded quadratic nonlinearities in quasi-phase-matched waveguides. *Opt. Lett.* **2018**, 43, 1678-1681.
7. McCarthy, J.E.; Bookey, H.T.; Psaila, N.D.; Thomson, R.R.; Kar, A.K. Mid-infrared spectral broadening in an ultrafast laser inscribed gallium lanthanum sulphide waveguide. *Opt. Express* **2012**, 20, 1545-1551.
8. Kubat, I.; Petersen, C.R.; Møller, U.V.; Seddon, A.; Benson, T.; Brilland, L.; Méchin, D.; Moselund, P.M.; Bang O. Thulium pumped mid-infrared 0.9–9μm supercontinuum generation in concatenated fluoride and chalcogenide glass fibers. *Opt. Express* **2014**, 22, 3959-3967.
9. Debord, B.; Alharbi, M.; Vincetti, L.; Husakou, A.; Fourcade-Dutin, C.; Hoenninger, C.; Mottay, E.; Gérôme, F.; Benabid, F. Multi-meter fiber-delivery and pulse self-compression of milli-Joule femtosecond laser and fiber-aided laser-micromachining. *Opt. Express* **2014**, 22, 10735-10746.
10. Maurel, B.; Delahaye, F.; Amrani, F.; Debord, B.; Gérôme, F.; Benabid F. 2-3 μm wavelength-range low-loss inhibited-coupling hollow-core fiber. *Paper of the Conference on Lasers and Electro-Optics U.S* **2018**, SF1K.2.
11. Yu, F.; Wadsworth, W.J.; Knight J.C. Low loss silica hollow core fibers for 3–4 μm spectral region. *Opt. Express* **2012**, 20, 11153-11158.
12. Yu, F.; Knight J.C. Negative curvature hollow-core optical fiber. *IEEE J. Sel. Top. Quantum Electron.* **2016**, 22, 146-155.

13. Adamu, A.I.; Habib, M.S.; Petersen, C.R.; Lopez, J.E.A.; Zhou, B.; Schülzgen, A.; Bache, M.; Amezcua-Correa, R.; Bang, O.; Markos C. Deep-UV to mid-IR supercontinuum generation driven by mid-IR ultrashort pulses in a gas-filled hollow-core fiber. *Sc. Reports* **2019**,9, 1-9.
14. Klimczak, M.; Dobrakowski, D.; Ghosh, A.; Stępniewski, G.; Pysz, D.; Huss, G.; Sylvestre, T.; Buczyński R. Nested capillary anti-resonant silica fiber with mid-infrared transmission and low bending sensitivity at 4000 nm. *Opt. Lett.* **2019**, 44, 4395-4398.
15. Cassataro, M.; Novoa, D.; Günendi, M.C.; Edavalath, M.N.; Frosz, M.H.; Travers, J.C.; Russell P.S.; Generation of broadband mid-IR and UV light in gas-filled single-ring hollow-core PCF. *Opt. Express* **2017**, 25, 7637-7644.
16. Michieletto, M.; Lyngsø, J.K.; Jakobsen, C.; Lægsgaard, J.; Bang, O.; Alkeskjold T.T. Hollow-core fibers for high power pulse delivery. *Opt. Express* **2016**, 24, 7103-7119.
17. Uebel, P.; Günendi, M.C.; Frosz, M.H.; Ahmed, G.; Edavalath, N.N.; Ménard, J.M.; Russell, P.S.J. Broadband robustly single-mode hollow-core PCF by resonant filtering of higher-order modes. *Opt. Lett.* 2016, **41**, 1961-1964.
18. Balciunas, T.; Fourcade-Dutin, C.; Fan, G.; T Witting, T.; Voronin, A.A.; Zheltikov, A.M.; Gerome, F.; Paulus, G.G.; Baltuska, A.; Benabid F. A strong-field driver in the single-cycle regime based on self-compression in a kagome fibre. *Nature Comm.* **2015**, 6, 1.
19. Köttig, F.; Novoa, D.; Tani, F.; Günendi, M.C .; Cassataro, C.; Travers, J.C., Russell P.S.J. Mid-infrared dispersive wave generation in gas-filled photonic crystal fibre by transient ionization-driven changes in dispersion. *Nature Comm.* **2017**, 8, 813.
20. Hasan M.I.; Akhmediev, N.; Mussot A.; Chang W. Midinfrared pulse generation by pumping in the normal dispersion regime of a gas filled hollow core fiber. *Phys. Rev. Appl.* **2019**, 12, 014050.
21. Ding, X.; Habib, M.S.; Amezcua-Correa, R.; Moses J. Near-octave intense mid-infrared by adiabatic down-conversion in hollow anti-resonant fiber. *Opt. Lett.* **2019**, 44, 1084-1087.
22. Hasan, M.I.; Akhmediev, N.; Chang W. Empirical Formulae for Dispersion and Effective Mode Area in Hollow-Core Antiresonant Fibers. *J. Lightw. Technol.* 2018, **36**, 4060-4065.
23. Marcatelli, E.A.J; Schmeltzer R.A. Hollow metallic and dielectric waveguides for long distance optical transmission and lasers. *Bell Syst. Tech. J.* 1964, **64**, 1783-1809.
24. Dudley, J.M.; Genty, G.; Coen, S. Supercontinuum generation in photonic crystal fiber. *Rev. Mod. Phys.* **2006**, 79, 1135-1184.
25. Matsubara, E.; Yamane K.; Sekikawa, T.; Yamashita M. Generation of 2.6 fs optical pulses using induced-phase modulation in a gas-filled hollow fiber. *J. Opt. Soc. Am. B* **2007**, 24, 985-989.
26. Fourcade-Dutin, C.; Imperio A.; Dauliat R.; Jamier R.; Muñoz-Marco H.; Pérez-Millán P.; Maillotte H.; Roy P.; Bigourd D. Temporal Distribution Measurement of the Parametric Spectral Gain in a Photonic Crystal Fiber Pumped by a Chirped Pulse. *Photonics* **2019**,6, 20.
27. Vanvincq O.; Fourcade-Dutin C.; Mussot, A.; Hugonnot, E.; Bigourd D. Ultrabroadband fiber optical parametric amplifiers pumped by chirped pulses. Part 1: analytical model. *J. Opt. Soc. Am. B.* **2015**, 32, 1479-1487.
28. Webb, K.E.; Xu, Y.Q.; Erkintalo, M.; Murdoch S.G. Generalized dispersive wave emission in nonlinear fiber optics. *Opt. Lett.* **2013**, 38, 151-153.
29. Robert, P.; Fourcade-Dutin, C.; Dauliat, R.; Jamier, R.; Muñoz-Marco, H.; Pérez-Millán, P. ; Dudley, J.M. ; Roy, P.; Maillotte, H.; Bigourd D. Spectral correlation of four-wave mixing generated in a photonic crystal fiber pumped by a chirped pulse. *Opt. Lett.* 2020, 45,4148-4151.